2011 NDIA GROUND VEHICLE SYSTEMS ENGINEERING AND TECHNOLOGY SYMPOSIUM
MODELING & SIMULATION, TESTING AND VALIDATION (MSTV) MINI-SYMPOSIUM
AUGUST 9-11 DEARBORN, MICHIGAN

EVOLUTION OF OCCUPANT SURVIVABILITY SIMULATION FRAMEWORK USING FEM-SPH COUPLING

Daniel Dooge
Ramesh Dwarampudi
ESI North America
Farmington Hills, MI

Grant Schaffner, PhD
Adam Miller
University of Cincinnati
School of Aerospace Systems
Cincinnati, OH

Ravi Thyagarajan, PhD
Madanmohan Vunnam
Venkatesh Babu
US Army, TARDEC
Warren, MI

ABSTRACT

To reduce the hazard for service personnel involved in current field operations, it is necessary to improve the safety and structural integrity of transport vehicles subjected to buried explosive material. Numerical simulation of the detonation effects of an Improvised Explosive Device (IED) on a vehicle and its occupants can provide tremendous value in this effort. Such events involve a range of complex phenomena at various dimensional and temporal scales, and it is not practical to capture all physical phenomena with just one single numerical method. A practical solution to this problem is proposed using a combination of Smoothed Particle Hydrodynamics (SPH) and Finite Elements.

Various numerical techniques have been proposed for simulating buried explosive over the past 30 years and this work has been previously described by many authors. However, the ability to define blast input parameters together with a soldier-centric simulation approach that includes human body and human-structural interactions with a vehicle subjected to an energetic effect poses a new challenge. SPH technology is a mesh-free Lagrangian method that can be configured with direct input of variables such as the soil density and explosive size without extensive tuning of parameters. The coupled SPH-FE approach is demonstrated for explosions and blast waves interacting with structures using a previously published validation study. For comparative purposes, the inclusion of Anthropomorphic Test Dummies (ATD's) to a vehicle model subjected to this blast load is presented under varying scenarios.

The PAM-SHOCK software allows combining SPH for the soil, detonation and blast wave propagation in a gaseous medium with Finite Elements for the structural dynamics of the vehicle and the occupant models and is presented in the current study. The proposed approach allows realistic and predictive simulations, based on realistic input, of vehicles and occupants subjected to IED blasts supportive of product development cycle constraints.

INTRODUCTION

Improvised Explosive Devices (IED's) have been responsible for 60% of coalition deaths in Iraq [1] (1,091 deaths Jan 2001 to Oct 2009 [2]) and 75% of casualties in Afghanistan [3] (614 deaths Oct 2001 to Oct 2009 [2]). In response, TARDEC has focused its philosophy towards survivability away from the conventional design-from-outside approach to a more occupant-centric approach, necessitated by threat changes in theater. The new philosophy starts with the person inside the vehicle and

works outward in the chain: soldier ⇨ seats ⇨ restraints ⇨ structure ⇨ crush zone ⇨ armor ⇨ shaping ⇨ standoff ⇨ energetic effect.

With the growing frequency of the use of improvised explosive devices (IEDs) throughout the world, efforts have been made to better understand how the released energy of these bombs interacts with surrounding structures. Even with modern computing power, detailed numerical modeling and simulation of structural response to blast loads are still extremely expensive and sometimes prohibitive. It has been common practice to compromise between simulation efficiency and simulation accuracy.

In past years a lot of research efforts have been spent either on improving the computational efficiency or accuracy of specific phases and features that constitute the blast event. Most of this research concentrated on simplifying the structures, such as reducing complex assemblies to an approximate reduced degree of freedom (DOF) system, evaluation of occupant seating independent of the vehicle environment, or using a substructure approach to model only part of the structure in detail. Although these approaches will yield valuable predictions under certain conditions, each of them has its associated assumptions and limitations. These assumptions and limitation are difficult to manage throughout the product development cycle and across non-congruent software in this piecewise development approach. Furthermore, these efforts are not well suited to predicting the sequence of blast-load to structural-response to human-vulnerability which is the focus of this paper.

In the recent military campaigns of Iraq and Afghanistan, the awareness of injuries incurred by service personnel has taken national spotlight leading to a renewed "soldier-centric" approach to vehicle design. In more recent work, the US Army [4] has begun to address the situation. The major evolution implemented in EPIC, which is a DoD code, is a particle method for a full Lagrangian based simulation. This same capability has been provided by the commercial domain PAM-SHOCK software. The additional benefit of the PAM solver framework includes a 15 year experience in refinement of coherent technologies including integrated support for a wide range of anthropoid representations in the form of arbitrary rigid bodies (ARB), anthropomorphic test devices (ATD's), and human models (H-model).

The motivation for this paper comes from interest within Research, Development and Engineering COMmand (RDECOM) to evaluate commercial off-the-shelf software applications relative to the vision of an end-to-end soldier centric occupant survivability solution. The methodology in the evaluation is described and compared to unclassified & published experimental data where available.

BLAST MODELING

It is well established that the numerical modeling of a blast event involves a range of complex phenomena. In particular, the introduction of a buried charge in soil presents additional complexity to an already complex event. The effectiveness of the IED is due to the way that the soil focuses energy towards the vehicle and into its structure and occupants. The vehicle survivability, its structural response, and response of the occupants, is affected by a complex set of interactions that occurs from the point of detonation to the response of the occupants in the vehicle. The complex sciences required for such an analysis include detonation chemistry, shock physics and soil mechanics, structural dynamics, nonlinear material behavior and human biomechanics.

Typically, for vehicle structural assessment and occupant survivability work we are primarily concerned with the loading and damage probability rather than the details of the explosive material detonation chemistry or soil mechanics. With this goal, the need and suitability for computational fluid dynamics and detailed soil fracture mechanics simulations in production work do not align.

The buried mine problem poses several challenges since the ejected material covering the charge imposes most of the loading onto the structure above. The properties of the material in the "soil cap" are therefore important, but they are modified by the time it hits the target. When looked at in detail, the processes modifying its properties are spalling, bulk cavitation, spherical spreading, and Richtmyer - Meshkov instability [5]. The standard numerical approach using Finite Elements is disadvantaged for these geo-material problems and often suffers from grid distortion problems [6]. To deal with these large deformation and material failure phenomena, the smoothed particle hydrodynamics (SPH) technique has been successfully applied to geo-material problems.

Soil-Blast Interaction

In our approach, the explosive material and the soil immediately surrounding the charge are represented by SPH elements.

The SPH option of the PAM solver has the capability to model continuum mechanics in Cartesian geometries in 1, 2 and 3 dimensions. For numerical simulation of continuum dynamics, the material is modeled by i = 1, 2, … N particles of mass m_i and density ρ_i. A particle i interacts with the neighboring particles j

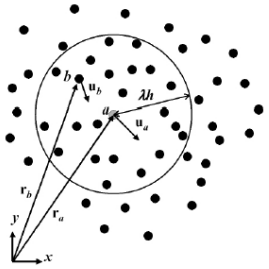

Figure 1: SPH sphere of influence

belonging to the sphere of influence of i. A sphere of influence (Fig. 1), is defined by a kernel function that weighs interactions and a smoothing length that limits interactions in space. Therefore, the integral interpolant of a function and its gradient can be approximated by a summation interpolant over a collection of particles:

$$\langle \varphi(\mathbf{r}_i) \rangle = \sum_j m_j \frac{\varphi_j}{\rho j} W(|\mathbf{r}_i - \mathbf{r}_j|, h) \quad (1)$$

$$\langle \nabla \varphi(\mathbf{r}_i) \rangle = \sum_j m_j \frac{\varphi_j}{\rho j} \nabla_i W(|\mathbf{r}_i - \mathbf{r}_j|, h) \quad (2)$$

Equation 2 shows that no mesh is required to numerically evaluate the gradient of the unknown functions since only the gradient of the (analytical) kernel function is required. The role of grid or mesh size in the Finite Difference Method or Finite Element Method is substituted by the particle size in SPH: a smaller particle size implies a better spatial resolution of the flow, but requires more CPU time. In practice, the smoothing length is usually defined to be proportional to the particle size [8].

The fact that SPH is a meshless method makes it attractive to simulating the dynamics of materials undergoing large relative displacements, while maintaining a Lagrangian frame of reference which enables one to track moving interfaces of virtually any shape.

Since the geometry and deformation of an SPH element (particle) is characterized by a single node, the number of particles to discretize a given volume may be taken roughly the same as the number of elements that would be used for a finite element distribution when using standard solid elements. Due to the assumption of a spherical smoothing kernel, the initial distance between adjacent particles in all directions should not differ too much. Hence, the aspect ratio for the solid elements from which the particles are usually generated should not become too big and it is recommended that it not exceed a factor of two. Although it is possible to define interacting particles with different size, a uniform distribution is recommended for particles representing a specific part.

A uniform distribution of closely packed particles will reduce any effects due to numerical re-distribution. For a non-uniform distribution, the smoothing length should be defined proportional to the particle radius, which is the default.

The interaction of the particles with the finite elements may be modeled by the existing sliding interface algorithms available within the PAM solver. The use of the contact algorithms between the smoothed particles and finite elements has been validated for a range of applications such as sloshing [9][10], heart valve opening [11] and impact of aeronautical structures on water [12].

The empirical Jones-Wilkins-Lee (JWL) equation of state is widely used in mine blast calculations and it is implemented in many simulation codes. The JWL Pressure-Volume relation is implemented in PAM-SHOCK in the following form:

$$p = A\left(1 - \frac{\omega}{R_1\, dF}\right)e^{-R_1\, dF} + B\left(1 - \frac{\omega}{R_2\, dF}\right)e^{-R_2\, dF} + \omega\frac{E_i}{V} \quad (3)$$

where P=pressure, V=relative volume, ω=Gruneisen parameter, C_v=heat capacity, and A, B, R_1, R_2 are material constants, dF =V/V_o, where V_o is the initial volume, V the current volume and E_i is the internal energy per unit volume [7]. The detonation starts from the ignition point. The detonation wave travels at a velocity D provided in the material data. The lightening time for an element is $\Delta t = d/D$, where d is the minimum distance between the element and the detonation point or line.

Reference Validation Set

A regularly cited work by Defence R&D Canada (DRDC) [13] was used as the preliminary validation set. In this experiment, a 182.88cm x 182.88cm (6' x 6') plate of Aluminum 5083-H131 armor was subjected to field trials of mine blasts. The main purpose of these tests was to provide data for validation of loading models.

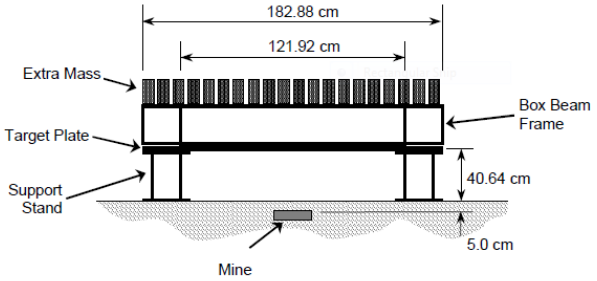

Figure 2: Schematic of DRDC experimental setup.

The Target Plate is supported on each corner by a Support Stand. A Box Beam Frame with additional mass was placed on top of the Target Plate. The Extra Mass was representative of the mass typical for a Light Armored Vehicle. The mine charge was specified in [13] as 6kg cylindrical charge of C4 explosive buried 50 mm below the surface of the soil.

The investigators also performed testing on rolled homogeneous armor (RHA) material but did not provide objective data in their results. Given this limitation, only the data for the aluminum plate were compared in the current study.

Blast Plate and Buried Mine Modeling

A model representing the experimental setup by the reference case [13] was built using the combined finite element and coupled SPH approach. A simplified view of the model setup is shown in Figure 3. A quarter model with symmetry boundary conditions was used to efficiently use

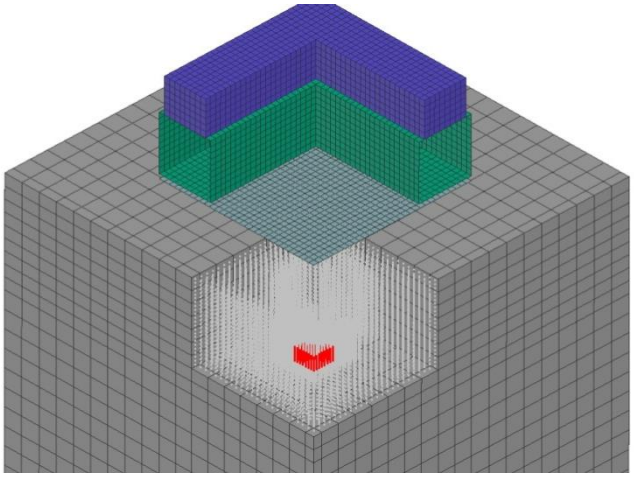

Figure 3: Model setup of DRDC experiment

computer time.

The deformable target plate material was represented by thin shell elements with five through-thickness integration points. A Belytschko-Tsay element formulation was selected with an aspect ratio of 1.0 in plane and 0.22 through the thickness. Despite the deviation away from thin shell theory recommended modeling practices regarding the thickness, this configuration of shell element and associated parameters were of interest over other element formulations particularly for application to everyday work tasks. The plate was constrained under gravity by weights added to the test frame.

The explosive charge was completely represented by SPH elements. A total of 448 SPH particles were uniformly distributed in the quarter volume radius of 127mm by 76.2mm with the ignition point defined at the center.

The properties for the explosive materials studied in the scope of this paper are presented in MKS units and summarized in Table 1. The properties for TNT are those from the reference test case [13]. As one of the goals for the study were to demonstrate that the physics of the problem are supported easily by realistic input values, we wished to investigate the plate response to C4 relative to commonly used scaled TNT properties. The values for parameters of the C4 EOS are from studies performed previously by ESI [16].

The overall soil was modeled by material extending unidirectional 1.8 meters and largely represented by solid elements with exception to a pit surrounding the buried explosive material. In this area where high distortion and chaotic displacements are experienced, the soil material in the immediate vicinity surrounding the explosive was modeled with 17,200 SPH particles comprising a space of 0.72m by 0.72m by 0.45m.

		TNT	C4
Density	Rho	1630	1601
First Constant in Pressure EOS	A	3.71E+11	5.98E+11
Second Constant in Pressure EOS	B	3.23E+09	1.38E+09
Third Constant in Pressure EOS	R1	4.15	4.5
Fourth Constant in Pressure EOS	R2	0.95	1.5
Fifth Constant in Pressure EOS	OMEGA	0.35	0.32
Detonation Velocity	D	6930	8040
Chapman-Jouget Pressure	pCJ	2.10E+10	2.81E+10
Initial Internal Energy / unit Volume	Eo	7.00E+09	8.70E+09

Table 1: Summary of JWL EOS parameters (M-K-S units)

Blast Plate Validation with Experimental Test

The evolution of charge ignition and soil deposition onto the target plate is shown in the following sequence of images. The particles shown in red color are representative of the TNT or C4 material. The key frame images show the rapid expansion of the explosive and soil cap ejection from the original ground location onto the surface of the plate. This progresses in a logical manner with the initial shock wave and then leads to increased mixing of media.

The momentum of the soil and explosive is transferred onto surrounding objects using an automatic contact definition.

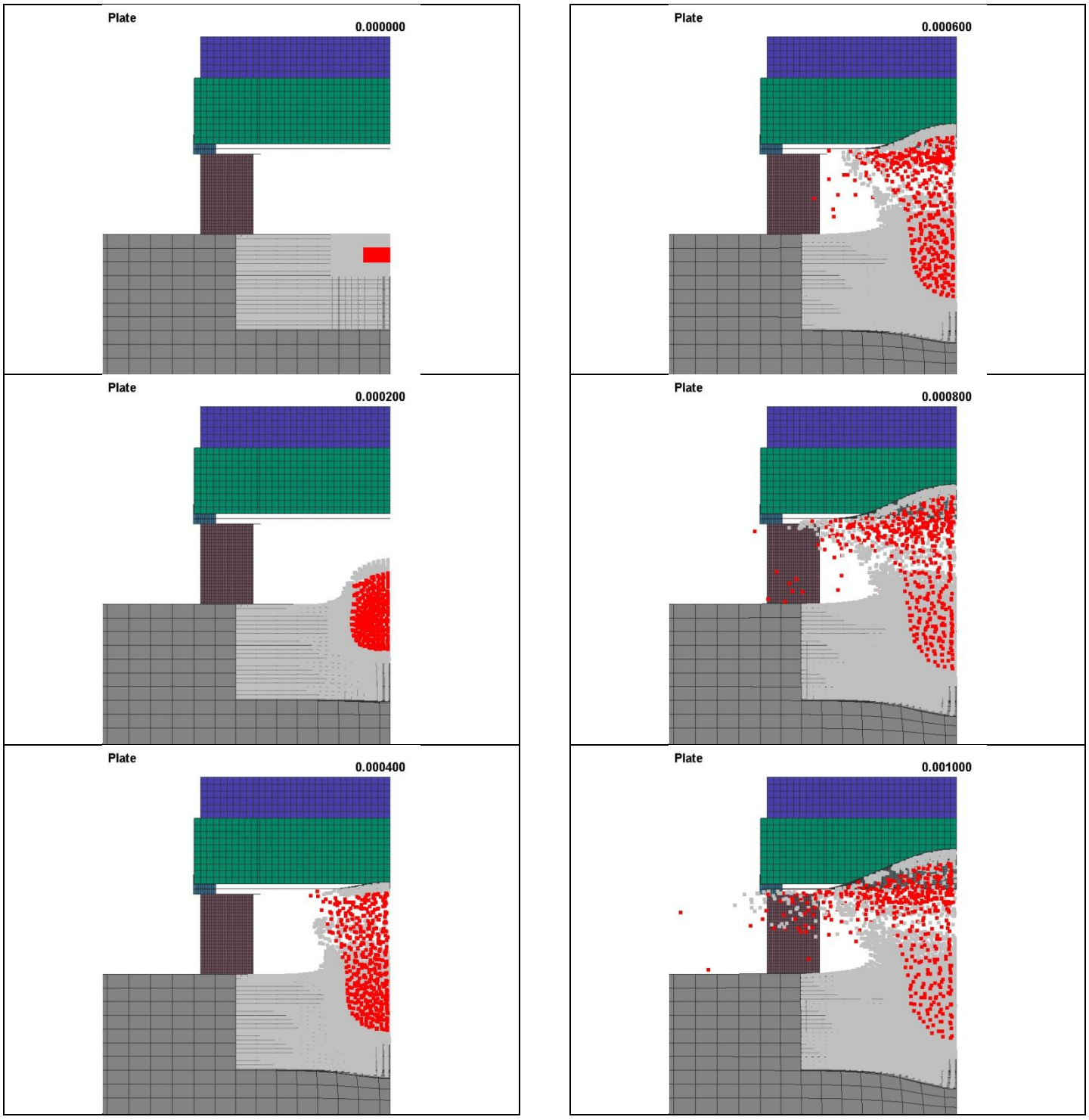
Plate
0.000000
Plate
0.000600
Plate
0.000200
Plate
0.000800
Plate
0.000400
Plate
0.001000

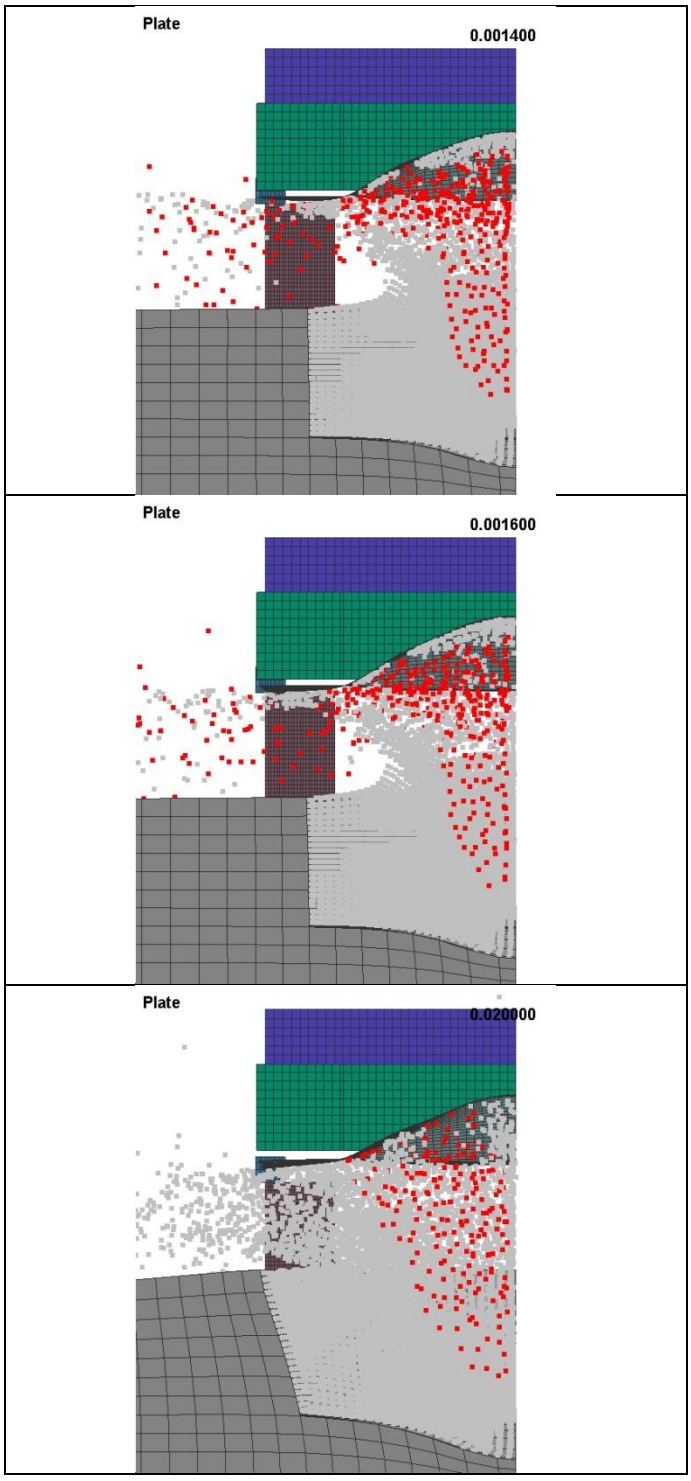

Figure 4: Keyframes of DRDC blast test

The resulting deformation typically looks like that shown in Figure 8. The deformation profiles show the difference in between DRDC and ESI soil definitions with rate-dependent plate properties reported by [17], to the aluminum plate tangent modulus provided by [13].

It was noted that the reference case did not provide any rate-dependent material properties, which may be of significance to the problem at hand. Following a hypothesis that the strain rate effect may play a role in the load-deformation characteristics, a literature search was performed. Similar research [17] was performed to characterize the same material under high strain rates. While the load mechanism of the experimental work [17] was different than that of a blast load, the data was used judiciously to verify the expected behavior.

Two of the strain rate curves, one from each extremity of the experimental results, were used in place of the basic

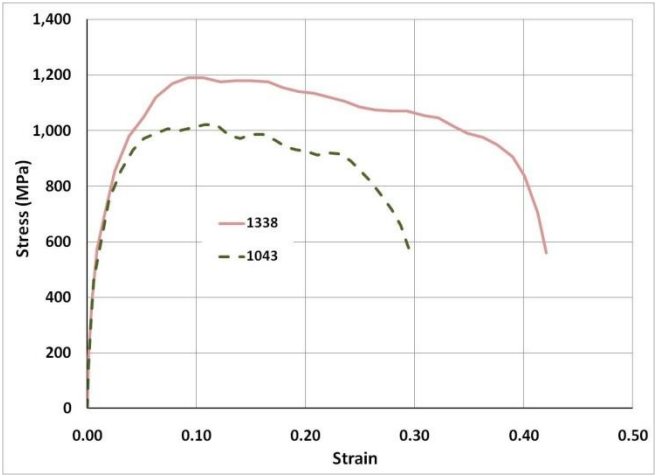

Figure 5: Stress strain curve properties of AL5083-H131 at rates of 1338/sec and 1043/sec.

material properties reported by [13]. It was found that the plate deformation profile did reduce with increased strain rate. One profile closely matching the reference experimental case is shown in Figure 6. The comparisons of the three material curves are shown in Figure 7. In the graph, the curve exhibiting the largest deformation (DRDC Soil_C4_Tangent) gradually reduced in magnitude with the strain rate effect. This finding supports the expectation and reinforces the need for this type of material characterization for this class of problems.

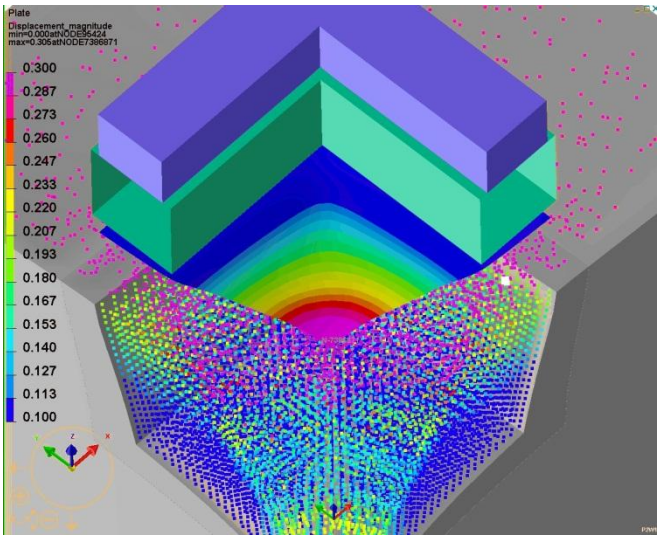

Figure 6: Deformation Profile using AL-H131 strain rates

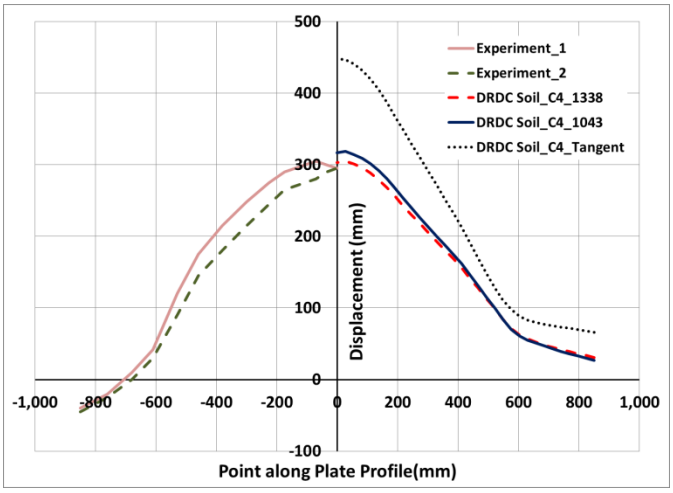

Figure 7: Comparison of plate deformation dependence on strain rate.

Blast Crater Observations

While the reference test case does not specifically list the type of soil used in the experimental test some properties were provided for numerical model studies. Literature review consistently reveals that soils exhibit a wide variety of properties and responses to various types of loading. In order to establish a basic level of understanding for the variance that may occur with different soil properties, a series of differing soil properties were studied.

The soil is represented using Material type 2, MAT_CRUSHABLE_FOAM, in PAM-SHOCK. The SPH discretization was not modified for any of the soil studies rather the properties were simply reassigned as seen in Table 2. Apart from the difference in density, shear and bulk modulus, the major difference between the DRDC and ESI soil material is the pressure cutoff for tensile fracture. With this parameter SPH particle will behave differently between the DRDC and ESI soil kinematics. The plots in Figure 8

Sim Label	*Density*	*Shear Modulus*	*Bulk modulus*
DRDC	2176	4.06E+10	5.00E+10
ESI	2500	1.48E+10	1.83E+11

Table 2: Soil properties evaluated by simulation (M-K-S units)

show the resulting deformed plate profile for each of the soil materials.

The images in Figure 9 show how varying soil properties can behave differently both in free flight and with interaction

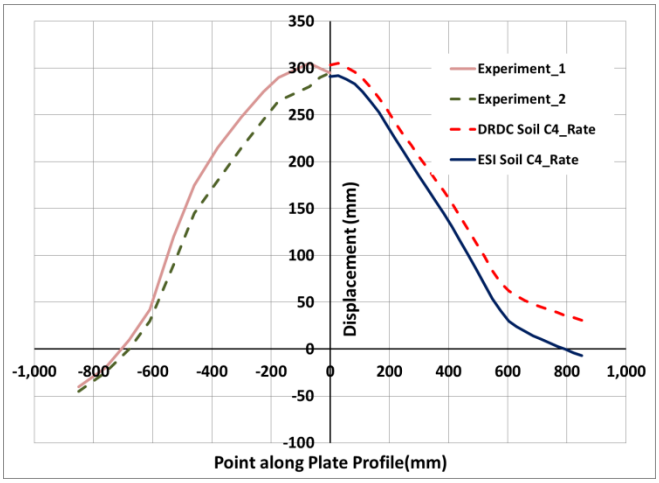

Figure 8: Comparison of predicted deformation for varying soil properties (symmetry plane of plate).

on surrounding structures. The upper image shows the behavior of the DRDC soil properties while the lower image shows the behavior of the ESI in which clumping of the particles occurs.

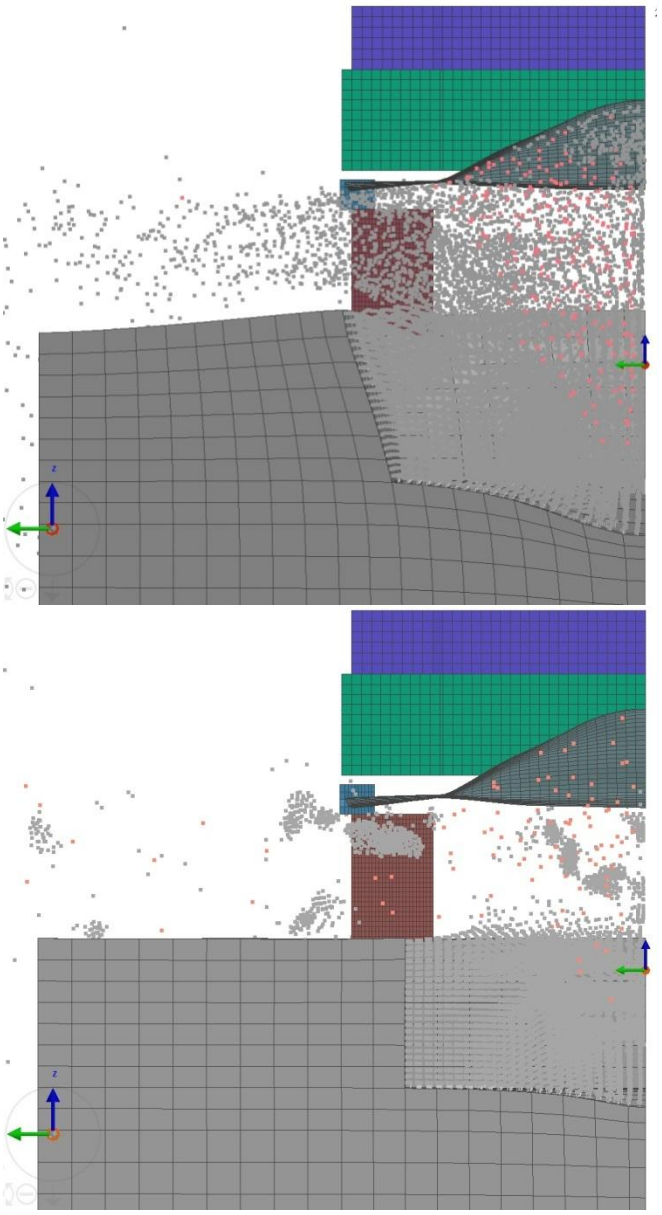

Figure 9: Comparison of soil kinematics between DRDC soil (upper) to ESI soil (lower)

VEHICLE MODELING & OCCUPANT RESPONSE

Many unclassified studies from past researchers have utilized fictitious vehicle geometry due to the unavailability of realistic information. Due to the sensitive nature of the work performed by the Department of Defense, data generated from testing military vehicles is usually classified, making it difficult to share data in the public domain.

In order to increase the operational relevance of studies performed by the wider scientific community, the US Army Tank Automotive Research, Development and Engineering Center (RDECOM-TARDEC) recently fabricated a generic vehicle hull with the intent to:

- Subject it to an underbody live fire test
- Share the data publicly
- Evaluate blast mitigation technologies

This effort has been described in detail [14] and continues to be analyzed and refined for industry consumption. This paper does not serve as the source for dissemination of these findings of the generic vehicle hull but does utilize a similar test configuration and vehicle geometry.

The experimental test setup of the generic hull is shown in

Figure 10: Experimental generic hull test

Figure 10. Six stands welded to the base of the structure provided simple supports and provided the appropriate standoff distance from the ground and the buried charge. The simplified vehicle structure's mass totaled 6,803 kg (15,000 lbs.). Center of gravity and inertia properties were not experimentally determined. The test preparation included a 12 foot by 12 foot by 5 foot plastic-lined pit filled with fully saturated play sand. The saturation was confirmed by standing water on top. Details of the mechanical soil properties, charge shape, dimensions, and depth of burial were not specifically re-created in this study.

The physical test was represented in the PAM-SHOCK modeling environment. The vehicle model shown in Figure 11 was set up with a ground clearance of 457 mm (18 inches). The explosive charge was representative of a generic STANAG 4569 Level 2 mine blast threat. The same blast model used earlier in this study for validation of previous work [13] was simply re-used in the full system model without modification.

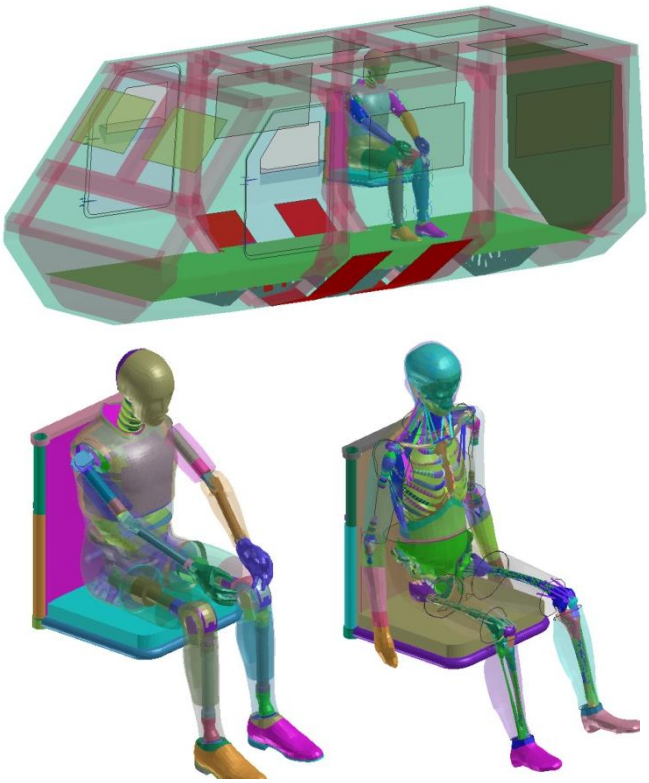

Figure 11: Model setup of generic hull test

Response Due to Acceleration Loading

In previous research, the Army has used a MADYMO model to estimate the risk of injury from blast events providing vertical acceleration loads ranging from 20g peak (30 ms duration) to 350g (5 ms duration) [15]. For this study, the generic hull model is subjected to 220g's of vertical acceleration pulse as shown in the curve of Figure 12. A portion of the generic hull shown in Figure 11 in red is defined as rigid. This rigid component is subjected to the acceleration pulse. Generic seat model is rigidly attached to the hull. Human and ATD models are positioned in the seat under gravity as show in Figure 11. Contact interactions are defined between human, seat and hull components. The occupant models are not restrained with seat belts.

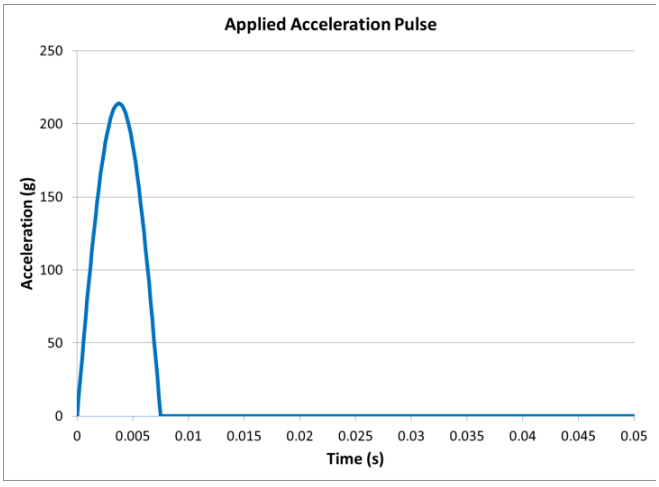

Figure 12: Enforced loading condition

Two types of occupant models were used in the simulations: an anthropometric test dummy (ATD) model based on the Hybrid III 50th%-ile family, and a human model with detailed representation of anatomical structures. This means that the human model has the following attributes: the head skull is deformable; each vertebra is a rigid body linked to its neighbors by kinematic joints; each scapula is a rigid body; ribs, sternum, clavicles and pelvic bones are deformable; each arm bone is a rigid body; leg bones are deformable; distal parts of the tibia and the fibula are included in one rigid body; each foot is a rigid body; organs are deformable; and skin and flesh are deformable. It may also be noted that another possible important feature, but not studied here, is that the failure models for the bones were not activated in these simulations. This level of detailed model is typically used for safety simulations aimed at giving access to kinematics and injuries.

The kinematic responses of the ATD and human models are compared in Figure 13. The models are shown with flesh representation in the left column, and with flesh removed in the right column for visualization of the skeletal structures (the flesh was still present in the simulation and both columns show the same simulation). The positioning of the models in the seat was similar but not identical due to the geometric differences of the models. Due to differences in the way the models are designed, the ATD spine is more curved (concave curvature toward models anterior) than the human model spine, particularly in the lumbar region when placed in the seated posture. The deformation of the flesh is quite noticeable, particularly in the waist and mid-thigh regions, and clearly more natural for the human model. Another noticeable and important difference in the model responses is the greater displacement and rotation of the ATD head relative to the human head, and the greater flexion in the ATD neck. There is also comparatively less deformation of the human spine compared to the ATD spine.

Comparisons of the ATD and human model results for pelvis acceleration, head acceleration, and tibia force are provided in Figures 14, 15 and 16, respectively. Due to the sensitive nature of these results, we are not able to provide absolute values for the parameters, but only relative comparisons between the dummy and human model.

In Figure 15, the human model shows a peak head acceleration approximately 70 % greater than the ATD and with the peak approximately 5 ms later in the human model. Beyond 40 ms, the two curves show closer correspondence. The peak pelvis acceleration (Figure 14) shows a reverse relationship between the human and ATD models, as

compared to the head acceleration. In this case, the peak pelvis acceleration for the human is approximately 50% of the peak pelvis acceleration for the ATD. As with the head, though, the human model response peak is about 5 ms later than the ATD peak. This delayed response remains consistent in the tibia load plots (Figure 16), but there is a very large difference in the initial peak force. For both the left and right leg, the ATD peak tibia force is approximately 6.5 to 7.5 times the peak force seen in the human tibia.

Figure 13: Comparison of kinematics between ATD and human model

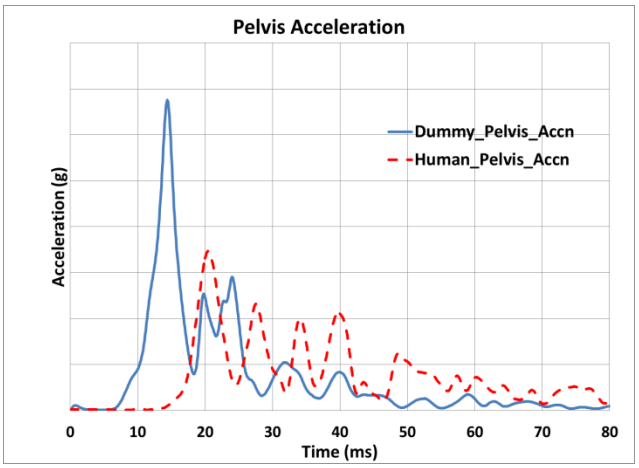

Figure 14: Comparison of pelvis acceleration

The differences in head acceleration, pelvis acceleration, and tibia force can be explained in terms of the differences in the models and with reference to Figure 13 (model kinematics and deformation renderings). The dummy model does not contain the detailed spine representation and distinction of different spine regions that the human model has. Also the human lumbar spine is more erect, which is natural for a seated posture. Furthermore, the human model spine, including the neck region, contains muscle representation, whereas the ATD does not. As a result, the ATD spine responds with lower stiffness than the human spine and does not represent the natural kinematics very well. These differences also explain why the peak head acceleration is lower for the ATD since the lower stiffness ATD spine provides less transmission of vehicle acceleration to the head.

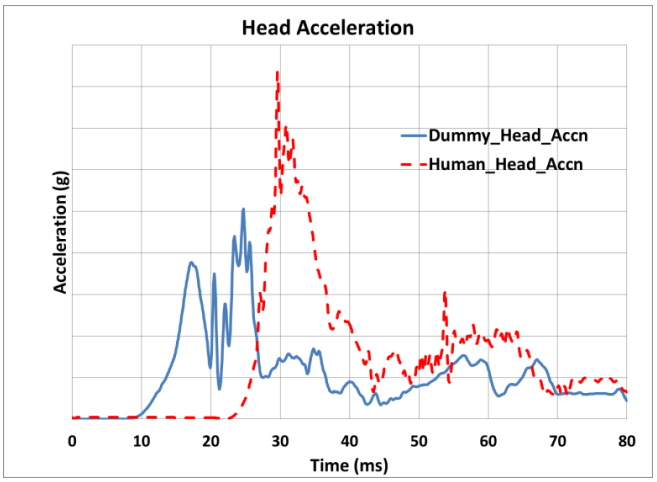

Figure 15: Comparison of head acceleration

The converse effect of higher pelvis acceleration for the ATD versus the human model is a result of material property differences that make the ATD pelvis stiffer than the human pelvis. The stiffness differences in the pelvis also explain the faster response and earlier peak of the pelvis acceleration for the ATD. This also drives the earlier peak in head acceleration for the ATD, although it is not clear why the stiffer spine in the human model does not appear to reduce the delay in response noticeably when acceleration is transmitted to the head.

The very large difference in tibia loading is a result of the differences in joint representation in the models, particularly that of the knee joint. In the ATD model, the knee is represented by kinematic joint, whereas the human model knee joint is represented using geometrical contacts with deformable ligament and muscle stabilization. As a result the human model knee joint is able to dislocate, whereas the ATD model knee joint is not able to dislocate. The

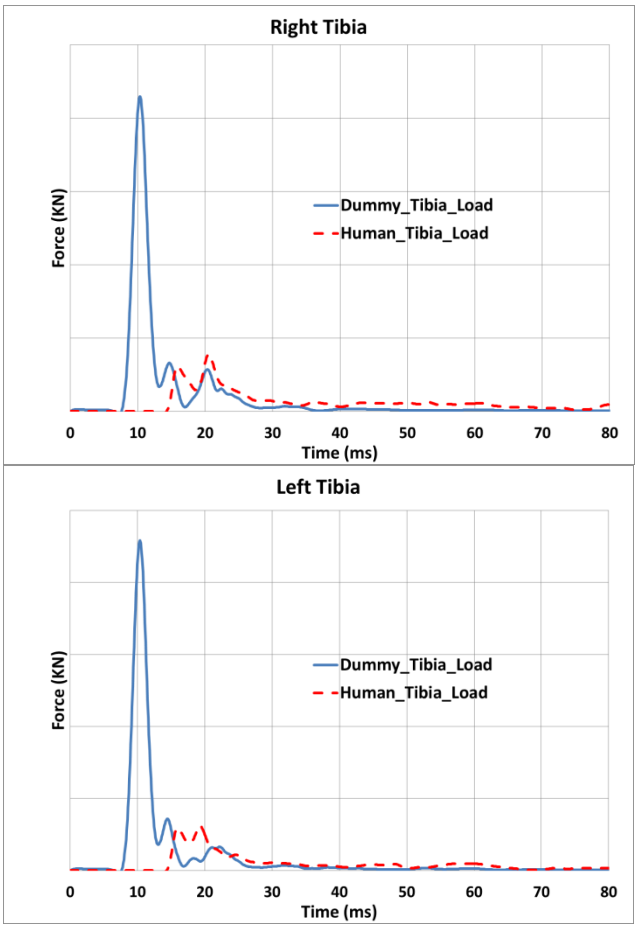

Figure 16: Comparison of tibia loads

dislocation of the human model knee, while representing a significant injury in itself, provides substantial energy dissipation and greatly reduces the reaction force on the tibia from the upper body inertia, resulting in the substantially lowered tibia force.

Blast Load Response on Deformable Vehicle

The vehicle model was positioned above a full three dimensional mine. The overall soil was modeled in the simulation over 3.65m by 3.65m by 1.72m (12 ft by 12 ft by 5.67 ft) deep area. The SPH particles comprised the inner 1.44m by 1.44m by 0.45m (4.7 ft by 4.7 ft by 1.5 ft) region

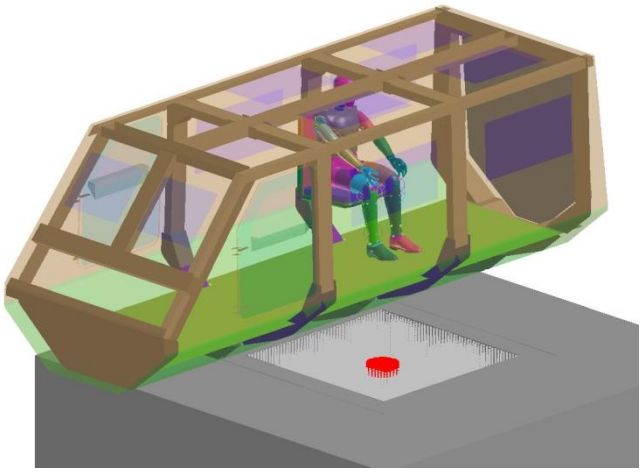

Figure 17: SPH blast loading under generic hull

where large displacements are expected.

In this section, the generic hull model is completely modeled as deformable. The loading applied on generic hull is provided by the blast impact of SPH particles. The blast represents a generic STANAG 4569 level 2 load. As shown in Figure 17, the charge is located at 457 mm (18 inches) from the bottom of the hull. The images of Figure 18, 19 & 20 show the hull deformation and blast event kinematics.

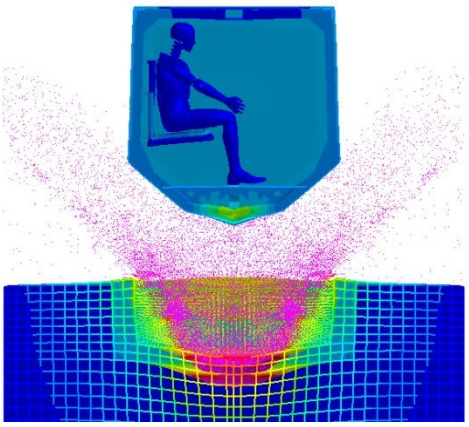

Figure 18: SPH blast loading under generic hull @ 10ms

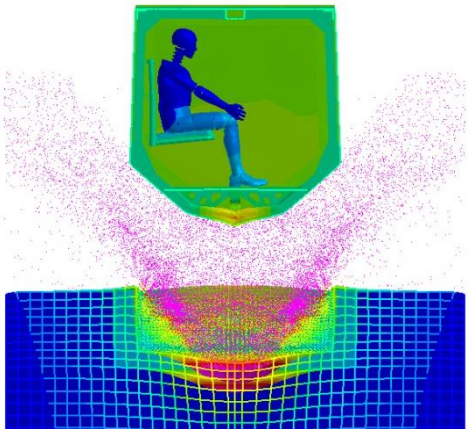

Figure 19: SPH blast loading under generic hull @ 30ms

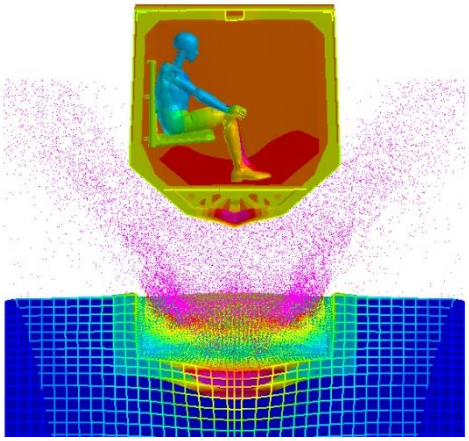

Figure 20: SPH blast loading under generic hull @ 50ms

Conclusions

The results reported here demonstrate a comprehensive approach towards occupant survivability simulations within a unified Lagrangian framework. This framework supports the vision for simplified modeling, intuitive input, realistic results and features in alignment with overall DoD tactical objectives. The methodology and tools identified are consistent with an occupant centric approach to vehicle design and development. The study used commercial off-the-shelf (COTS) software to demonstrate preliminary results from coupled fluid-structure interaction simulations.

The human model kinematics presented are more realistic than ATD models due to better bio-fidelic representation of body segments. Further work is needed in detail to validate tissue and structure response of human models under high acceleration blast type loads.

The PAM-SHOCK coupled Finite Element to SPH approach was demonstrated for explosions and blast waves interacting with structures. Results were compared to previously published data with good correlation.

The complete occupant centric framework was demonstrated including standard and advanced occupant models coupled with vehicle structural analysis and energetic effects was then demonstrated. Data from a generic hull test was used for this demonstration although a full correlation study was not performed.

REFERENCES

[1] C. Wilson, "Improvised Explosive Devices (IEDs) in Iraq and Afghanistan: Effects and Countermeasures", CRS Report for Congress, RS22330, August 28, 2007.

[2] S. Bird and C. Fairweather, "Recent military fatalities in Afghanistan (and Iraq) by cause and nationality", MRC Biostatistics Unit, UK, February 2010.

[3] J Farago, "IED Casualties in Afghanistan Soaring", http://www.newser.com/story/55161/ied-casualties-in-afghanistan-soaring.html, 3 April. 2009.

[4] K. Danielson, et. al, "Lagrangian Meshfree Methodologies For Predicting Loadings From Buried Munitions Detonations", 27th Army Science Conference.

[5] L. Taylor, et. al, "Loading Mechanisms from Shallow Buried Explosives", 24th International Symposium on Ballistics, New Orleans, LA, 2008.

[6] H. Bui, et. al, "SPH-Based Numerical Simulations for Large Deformation of Geomaterial Considering Soil-Structure Interaction", The 12th International Conference of International Association for Computer Methods and Advances in Geomechanics (IACMAG), October, 2008, Goa, India.

[7] ESI Group, "Virtual Performance Solution: Solver Notes Manual", 2008.

[8] ESI Group, "Virtual Performance Solution: Solver Reference Manual", 2008.

[9] M. Meywerk, F. Decker, and J. Cordes, "Fluid-structure interaction in crash simulation.", Proc. Inst. Mech. Engrs. 214,669–673., 1999.

[10] H. Cha, et. al, "Industrial applications of PAM-SHOCK using SPH", PAM Users. Proc. Conf. Korea HANPAM '99, 253–265 Seoul, November 15–16, 1999.

[11] C. Haack, "On the use of a particle method for analysis of fluid-structure interaction.", Sulzer Innotech Report STR_TB2000_014, 2000.

[12] H. Climent, et. al, "Aircraft ditching numerical simulation", Proc. 25th Int. Congress of the Aeronautical Sciences, Hamburg, Germany, 2006.

[13] K. Williams, et. al, "Validation of a Loading Model for Simulating Blast Mine Effects on Armoured Vehicles", 7th International LS-DYNA Users Conference.

[14] R. Scherer, "Vehicle and Crash-Dummy Response to an Underbelly Blast Event", 54th Stapp Conference (Oral Only).

[15] S. Arepally, et. al, "Application of Mathematical Modeling in Potentially Survivable Blast Threats in Military Vehicles", 26th Army Science Conference, Orlando, Florida, 2008.

[16] A. Kamoulakos, et. al, "Finite Element Modelling of Fluid/Structure Interaction in Explosively Loaded Aircraft Fuselage Panels using PAMSHOCK / PAMFLOW Coupling", Presented at the Conference on Spacecraft Structures, Materials and Mechanical Testing ESA/CNES/DARA, Noordwijk, The Netherlands, 27-29 March 1996

[17] M. Bassim, "High Strain Rate Evaluation of Armor Materials", DRDC Valcartier CR 2007-266